

Phase Inversion of Polybutadiene/Polyisoprene Blends under Quiescent and Shear Conditions

H. S. Jeon*

Department of Petroleum & Chemical Engineering, New Mexico Institute of Mining and Technology, Socorro, New Mexico 87801

A. I. Nakatani, E. K. Hobbie, and C. C. Han

Polymers Division, National Institute of Standards and Technology, Gaithersburg, Maryland 20899

Received August 11, 2000. In Final Form: January 24, 2001

We investigate the effect of phase inversion on the domain morphology and rheological properties of phase-separated polybutadiene/polyisoprene blends using optical microscopy, light scattering, and rheometry. Two different blends, low-vinyl polybutadiene/low-vinyl polyisoprene (LPB/LPI) and low-vinyl polybutadiene/high-vinyl polyisoprene (LPB/HPI), were used in this study. The LPB/LPI blend has a lower critical solution temperature (LCST) of $(62 \pm 1)^\circ\text{C}$, while the LPB/HPI blend exhibits upper-critical-solution-temperature (UCST) behavior with a critical temperature above the experimentally accessible temperature window. We determine the quiescent phase-inversion composition ($\phi_{\text{LPI}} = 0.55 \pm 0.05$) of phase-separated LPB/LPI blends from the discontinuity in the dynamic storage modulus and shear viscosity. For LPB/HPI, we find that a shear-induced coexisting structure (apparent as a “walnutlike” light-scattering pattern) develops at a fixed composition ($\phi_{\text{HPI}} = 0.8$) and constant temperature. The coexisting morphology consists of two different anisotropic structures; stringlike domains and small ($\xi < 5 \mu\text{m}$) vorticity-aligned domains. We suggest that shear-induced phase inversion may lie at the foundation of this effect, although more theoretical and experimental work is needed to verify this.

Introduction

Phase inversion in two-phase polymer mixtures is a key factor that can influence domain morphology in a number of practical applications, such as biomedical materials, cosmetics, foods, membranes, separations, and polymerization technologies.^{1–11} Traditionally associated with emulsions, in which there are two immiscible phases (dispersed and continuous), phase inversion occurs when the dispersed phase is converted into a continuous phase due to changes in concentration, temperature, and/or shear forces. Paul and Barlow,¹² Jordhamo et al.,¹³ and Miles and Zurek¹⁴ have proposed an empirical equation that predicts the point at which phase inversion will occur in terms of a dimensionless parameter α :

$$\alpha = \frac{\phi_A \eta_B(\dot{\gamma}, T)}{\phi_B \eta_A(\dot{\gamma}, T)} \quad (1)$$

where ϕ_i is the volume fraction of component i ($i = \text{A or B}$) and η_i represents the viscosity of component i at a given shear rate ($\dot{\gamma}$) and temperature (T). This equation implies that the viscosity and composition ratio of the two components determines the phase-inversion point. If $\alpha > 1$, the B-rich phase is dispersed, while if $\alpha < 1$, the A-rich phase is dispersed. If the viscosity ratio is balanced by the composition ratio ($\alpha \sim 1$), then phase inversion may occur under either quiescent or shear conditions. Phase inversion in polymer blends, which often have an emulsion-like morphology, is not as well understood as it is in microemulsions. Several studies have demonstrated that eq 1 has validity, both for blends with viscosity ratios close to unity^{13–17} and for blends at low shear rates.^{15,18–19} In contrast, eq 1 does not quantitatively predict the correct phase-inversion point for systems that exhibit viscoelastic asymmetry between the melt components.^{3,5,20}

In general, the morphology of polymer blends is affected by such things as the processing conditions, the composition, and the viscoelastic properties of both phases, as well as the interfacial tension between them. Equation 1 implies that phase inversion depends not only on thermodynamic variables (such as volume fraction and tem-

* To whom correspondence should be addressed.

(1) Akay, G. *Chem. Eng. Sci.* **1998**, *53*, 203. Akay, G. *Polym. Eng. Sci.* **1994**, *34*, 865.

(2) Tanaka, H.; Araki, T. *Phys. Rev. Lett.* **1997**, *78*, 4966.

(3) De Roover, B.; Devaux, J.; Legras, R. *J. Polym. Sci., A: Polym. Chem.* **1997**, *35*, 917.

(4) Mekhilef, N.; Verhoogt, H. *Polymer* **1996**, *37*, 4069.

(5) Utracki, L. A. *J. Rheol.* **1991**, *35*, 1615.

(6) Wu, S. H. *Polym. Eng. Sci.* **1987**, *27*, 335.

(7) Hsieh, K. H.; Woo, E. M. *J. Polym. Sci., B: Polym. Phys.* **1996**, *34*, 2591.

(8) Barton, B. F.; Reeve, L. L.; McHugh, A. J. *J. Polym. Sci., B: Polym. Phys.* **1997**, *35*, 569.

(9) Utracki, L. A. *Polymer Alloys and Blends*; Hanser Publishers: New York, 1990.

(10) Han, C. D. *Rheology in Polymer Processing*; Academic Press: New York, 1976.

(11) Han, C. D. *Multiphase Flow in Polymer Processing*; Academic Press: New York, 1981.

(12) Paul, D. R.; Barlow, J. *J. Macromol. Sci., Rev. Macromol. Chem.* **1980**, *C18*, 109.

(13) Jordhamo, G. M.; Manson, J. A.; Sperling, L. H. *Polym. Eng. Sci.* **1986**, *26*, 517.

(14) Miles, I. S.; Zurek, A. *Polym. Eng. Sci.* **1988**, *28*, 796.

(15) Bouilloux, A.; Ernst, B.; Lobbrecht, A.; Muller, R. *Polymer* **1997**, *38*, 4775.

(16) Levij, M.; Maurer, F. H. *Polym. Eng. Sci.* **1988**, *28*, 670.

(17) Zhang, X.; Yin, Z.; Yin, J. *J. Appl. Polym. Sci.* **1996**, *62*, 893.

(18) Ho, R. M.; Wu, C. H.; Su, A. C. *Polym. Eng. Sci.* **1988**, *30*, 511.

(19) Hietaoja, P. T.; Holsti-Miettinen, R. M.; Seppala, J. V.; Ikkala, O. T. *J. Appl. Polym. Sci.* **1994**, *54*, 1613.

(20) Favis, B. D.; Chalifoux, J. P. *Polymer* **1988**, *29*, 1761.

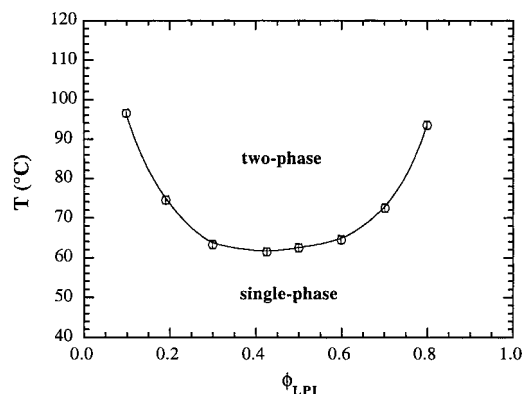


Figure 1. Measured phase diagram of the LCST LPB/LPI blend.

perature) but also on hydrodynamics via the shear viscosity. The purpose of the present work is to study the effects of blend composition and shear rate on phase inversion and domain morphology in phase-separated polymer blends. We find that the phase-inversion composition coincides with a discontinuity in the shear viscosity and dynamic storage modulus. Moreover, the phase-inversion composition determined from microscopy and rheometry agrees well with the value predicted from theory. We also find a novel coexisting structure (apparent as a “walnutlike” light-scattering pattern) that develops due to a shear-induced phase inversion at a fixed composition and a constant temperature.

Experimental Section

Materials. The polymers used in this study were synthesized at Goodyear Tire and Rubber Company.²¹ The number-averaged relative molecular mass (M_n), the mass-averaged relative molecular mass (M_w), and the polydispersity were determined by gel permeation chromatography (Waters Model 150-C), and the microstructure was probed using ¹³C nuclear magnetic resonance (NMR). The polybutadiene and polyisoprene chains are statistical copolymers, composed of 1-4, 1-2 isomers and 1-4, 3-4 isomers, respectively. The polybutadiene has a mole fraction of 1-2 isomers equal to 0.1 (denoted LPB), while the two polyisoprenes have mole fractions of 3-4 isomers equal to 0.07 (denoted LPI) and 0.9 (denoted HPI). The polymer characteristics are summarized in Table 1.

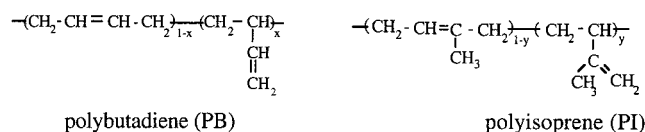
Table 1. Polymer Characteristics

polymer	label	vinyl content	M_n	M_w/M_n	η'_{0^a}	M_e^b
		%	g/mol		P	g/mol
1,4-polybutadiene	LPB	10	51 000	1.04	2300	4 200
1,4-polyisoprene	LPI	7	88 000	1.08	6900	10 600
3,4-polyisoprene	HPI	90	72 000	1.02	19700	13 100

Table 2. Blend Characteristics^e

blend	type	ϕ_{LPI} or ϕ_{HPI}	R^c (μm)	η'_{0^a} (P)	T_C ($^{\circ}\text{C}$)	λ^d
B10	LPB/LPI	0.102	1.93 ± 0.08	2560	96.5 ± 0.5	3.0
B20	LPB/LPI	0.204	4.54 ± 0.14	3150	74.5 ± 0.5	3.0
B30	LPB/LPI	0.306	9.03 ± 0.77	3550	64.5 ± 0.5	3.0
B40	LPB/LPI	0.408	11.50 ± 1.04	3910	61.5 ± 0.5	3.0
B50	LPB/LPI	0.500	11.77 ± 1.32	4310	62.0 ± 0.5	3.0
B60	LPB/LPI	0.602	13.69 ± 1.16	4540	65.5 ± 0.5	0.33
B70	LPB/LPI	0.714	8.97 ± 0.57	4840	72.5 ± 0.5	0.33
B80	LPB/LPI	0.816	3.32 ± 0.11	5300	93.5 ± 0.5	0.33
B90	LPB/LPI	0.918	< 1.0	6860		0.33
A20	LPB/HPI	0.199	6.22 ± 1.5	3640	> 180	8.6
A40	LPB/HPI	0.448	13.4 ± 3.7	4750	> 180	8.6
A80	LPB/HPI	0.802	3.40 ± 0.4	15500	> 180	0.12

^a The dynamic zero-shear viscosity of homopolymers and blends was obtained by averaging over plateau values of viscosity at a wide range of frequency at 130 $^{\circ}\text{C}$. ^b The entanglement molecular weight was determined from the plateau modulus of homopolymers. ^c The number-average droplet radius in the dispersed phase at 130 $^{\circ}\text{C}$ was obtained by averaging 23–58 droplets per sample. ^d The viscosity ratio was obtained from the dynamic zero-shear viscosity at 130 $^{\circ}\text{C}$. ^e The uncertainties in quoted numerical results represent the estimate of the standard error in experimental uncertainty



Samples. The low-vinyl polybutadiene/low-vinyl polyisoprene (LPB/LPI) and low-vinyl polybutadiene/high-vinyl polyisoprene (LPB/HPI) blends used in this study were prepared via solution blending. We started with a dilute solution (mass fraction 0.02 total polymer) containing the appropriate amount of each component and a small amount (mass fraction 0.0005) of Goodyear Wingstay #29 antioxidant in a solvent of methylene chloride. The mixture was stirred at room temperature for 1 day and filtered through a 0.45 μm Gelman Acrodisc CR PTFE filter.

50 μm

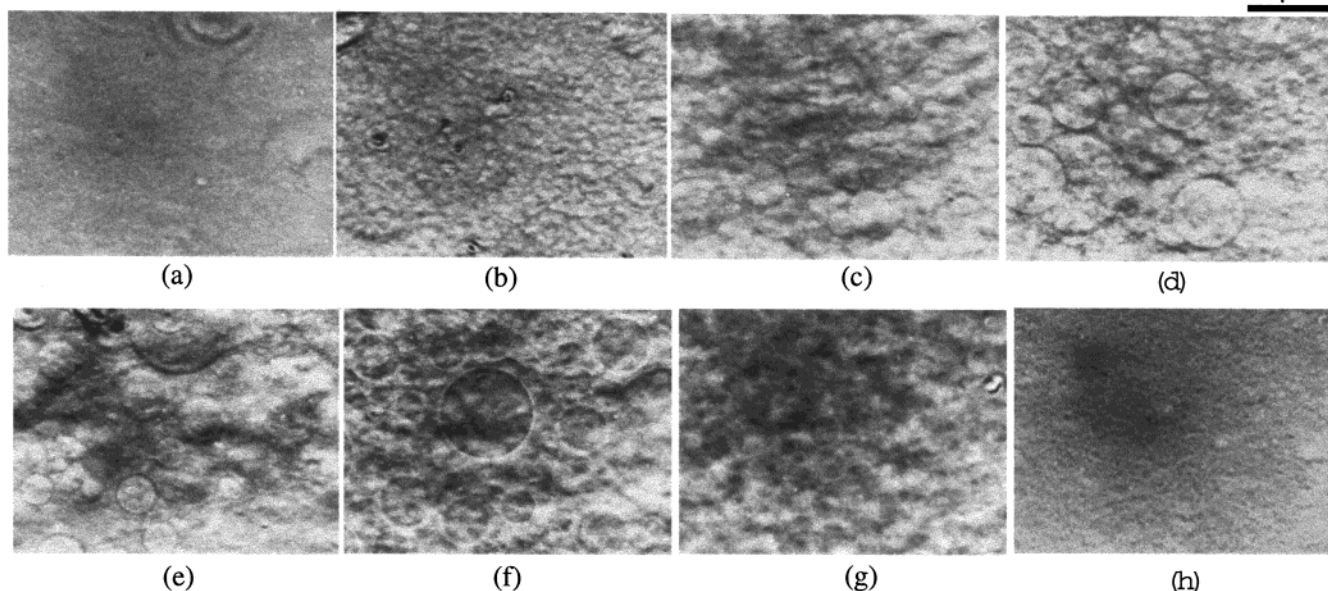


Figure 2. Optical micrographs for the LPB/LPI blends under quiescent conditions at 130 $^{\circ}\text{C}$: (a) B10; (b) B20; (c) B30; (d) B40; (e) B50; (f) B60; (g) B70; (h) B80.

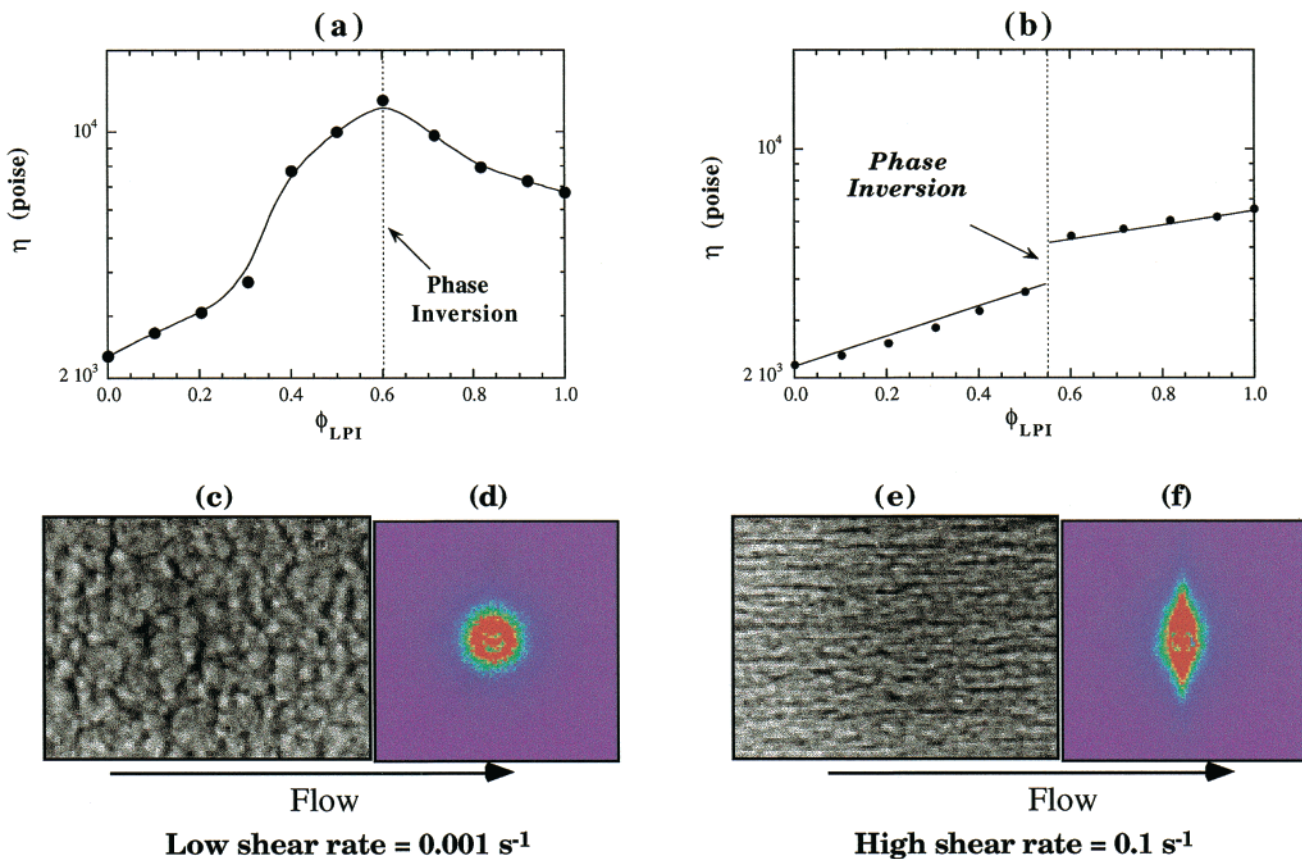


Figure 3. Steady-shear viscosity of LPB/LPI versus ϕ_{LPI} at 130 °C for shear rates of (a) 0.001 s^{-1} [as shown in parts c and d, the domain shape for a B40 blend at this shear rate is spherical] and (b) 0.1 s^{-1} [as shown in parts e and f, the domain shape for a B40 blend at this shear rate is elongated, stringlike droplets]. The width of each micrograph is 200 μm , and the scattering pattern subtends an angle of 27°.

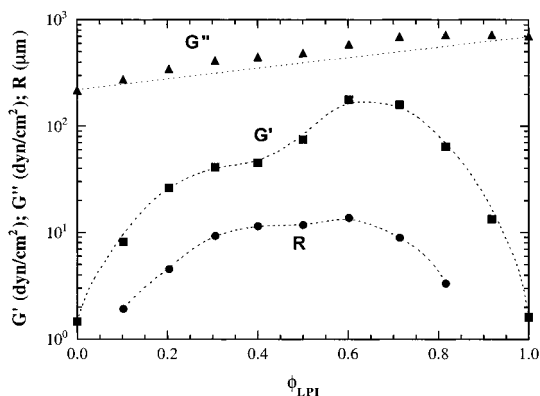


Figure 4. Compositional dependence of the dynamic storage modulus, the dynamic loss modulus (both measured at 0.1 rad/s), and the mean droplet radius for phase-separated LPB/LPI blends at 130 °C, where the straight line is the prediction of the log-additive mixing rule.

The solvent was then evaporated under an atmosphere of flowing nitrogen gas, and the sample was dried in a vacuum oven at room temperature for several days before measurements were performed. The LPB/HPI and LPB/LPI blends are labeled A_{xx} and B_{yy} , respectively, where xx is the volume percent of HPI and yy is the volume percent of LPI in the blends. The exact compositions and designations of the blends used in this study are given in Table 2. All experiments were performed at a constant temperature of 130 °C, where the blends show phase-separated structures under quiescent conditions. The LPB/LPI sample was heated from room temperature to 130 °C and held for 120 min under quiescent conditions to obtain a reproducible initial two-phase morphology for each sample. In contrast, the LPB/HPI sample was heated from room temperature to 130 °C and held

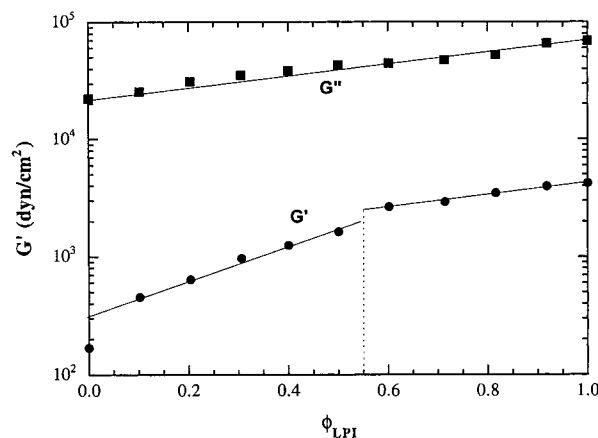


Figure 5. Compositional dependence of the dynamic storage modulus and the dynamic loss modulus at a frequency of 10 rad/s for phase-separated LPB/LPI blends at 130 °C. The phase inversion point is evident as a discontinuity in the storage modulus.

for 240 min under low shear rate ($\dot{\gamma} = 0.005 \text{ s}^{-1}$) to obtain a reproducible initial two-phase morphology for each sample.

Light Scattering and Optical Microscopy. The in-situ light scattering and optical microscopy instrument, capable of collecting two-dimensional light scattering data and real-time microscopy images, was designed and constructed for conducting optical measurements on two-phase systems under simple shear flow. The sample compartment is composed of two electrically heated quartz plates, and the temperature of each plate is controlled to within $\pm 0.5 \text{ K}$ by a 100 Ω platinum-resistance-temperature-detector (RTD) element in conjunction with a 1 mA constant-current source. The gap distance between parallel

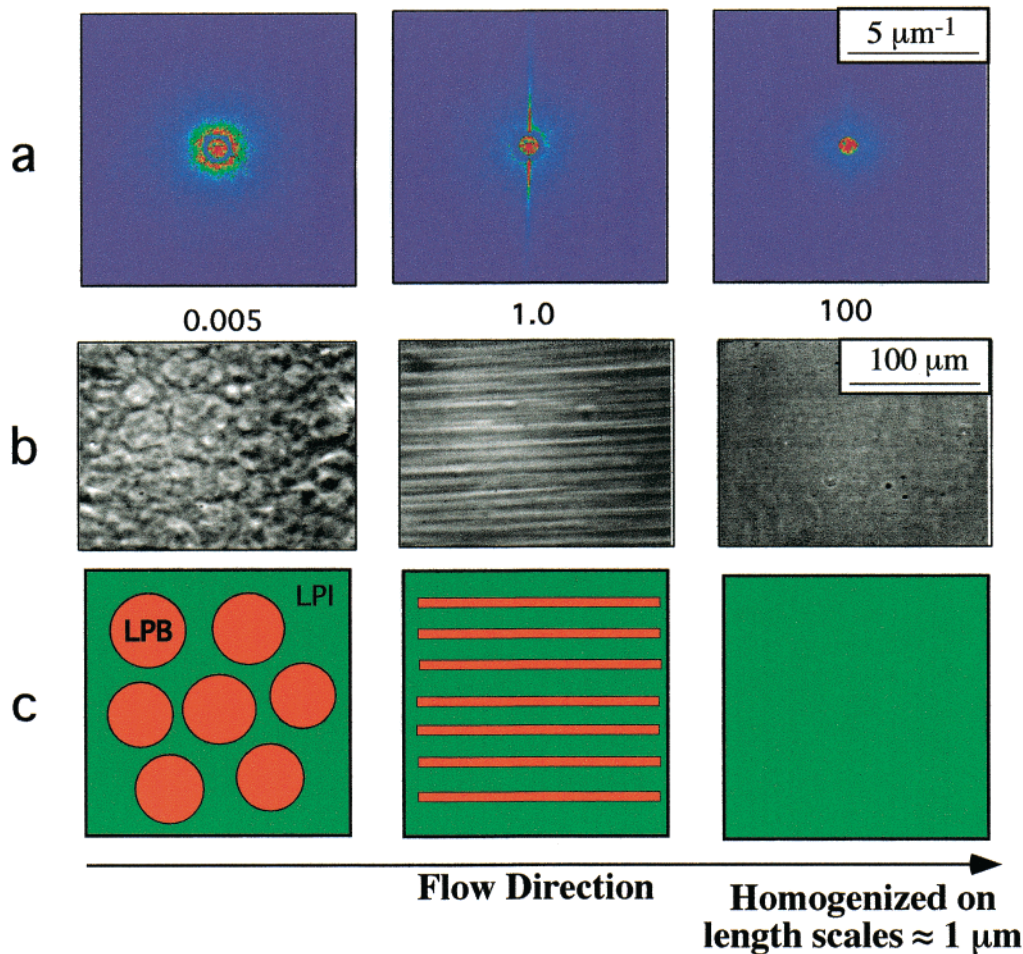


Figure 6. (a) Two-dimensional small-angle light-scattering (SALS) patterns, (b) phase-contrast optical micrographs, and (c) domain morphology cartoons for the B60 blend at 130 °C at various shear rates, where the shear rate in inverse seconds is indicated under each light-scattering pattern. The flow direction is from left to right, and the vorticity direction is from top to bottom.

quartz plates was fixed at 465 μm for all rheo-optical experiments. A beam of vertically polarized monochromatic light from a 15 mW He–Ne laser (wavelength $\lambda = 632.8$ nm) was directed through the sample. The image of the scattered light in the angular range $4\text{--}27^\circ$ [corresponding to wave vector (q) values ranging from 0.69 to 4.64 μm^{-1}] was focused onto a thermoelectrically cooled two-dimensional charge-coupled-device (CCD) detector using a pair of spherical condensers, and the array of data from the 256 pixel \times 256 pixel CCD camera was then transferred to a personal computer. In contrast, the microscope image is collected with a different CCD camera (Dage MTI, model 72), recorded onto a super-VHS tape, and digitized using a frame grabber from Data Translation (DT 3851). The geometry of the instrument is such that it probes structures within the plane defined by the flow and neutral (or vorticity) directions. A detailed description is given elsewhere.²²

The phase-separation temperature of the blend was determined by phase-contrast optical microscopy. Conventional bright-field microscopy relies on a significant refractive index difference between the phases in the sample to resolve the image. In the case of phase-separated PB/PI blends, it is difficult to obtain a well-resolved image with bright-field microscopy because the refractive index difference between the two components is very small ($n_{\text{LPB}} = 1.512$ and $n_{\text{LPI}} = 1.517$).²³ Therefore, a phase-contrast optical microscope is required. An advantage of this small optical contrast, however, is that multiple scattering effects

are suppressed when light scattering is used to probe the morphology over smaller length scales.

Rheometer. A Rheometrics Scientific SR-5000 rheometer was utilized in a parallel-plate geometry for oscillatory- and steady-shear measurements, which were carried out with 25 mm diameter fixtures and a (0.4 ± 0.01) mm gap thickness. The temperature was controlled to within ± 0.5 K, and the measurements were carried out under a nitrogen atmosphere to prevent any thermal degradation of the polymers, which are known to be sensitive to heat. To study the linear viscoelasticity, oscillatory-shear measurements were performed at various frequencies ($0.1 \text{ rad/s} \leq \omega \leq 100 \text{ rad/s}$) in a constant-strain mode using small-strain-amplitude ($\gamma_0 = 0.08$) conditions. The dynamic zero-shear viscosity was obtained by averaging over plateau values of viscosity at a wide range of frequency at 130 °C. The dynamic storage (G') and loss (G'') moduli of the phase-separated LPB/LPI blends were measured at various frequencies (0.1, 1, 10, and 100 rad/s).

Results and Discussion

1. Phase Diagram. The phase-transition temperature of the LPB/LPI blends was determined by phase-contrast optical microscopy using a step heating method.²⁴ The prepared blend sample was heated in 5 K increments and then allowed to anneal for 120 min. Near the transition temperature, the intervals were reduced to 2 K for greater accuracy. Phase separation was apparent as the formation

(21) Certain commercial equipment, instruments, or materials are identified in this article in order to adequately specify the experimental procedure. Such identification does not imply recommendation or endorsement by the National Institute of Standards and Technology, nor does it imply that the materials or equipment identified are necessarily the best available for the purpose.

(22) Kim, S.; Yu, J. W.; Han, C. C. *Rev. Sci. Instrum.* **1996**, *67*, 3940.

(23) Brandrup, J.; Immergut, E. H., *Polymer Handbook*, 3rd ed.; Wiley-Interscience: New York, 1989; Chapter IV, p 455.

(24) Sung, L.; Hess, D. B.; Jackson, C. L.; Han, C. C. *J. Polym. Res.* **1996**, *3*, 139.

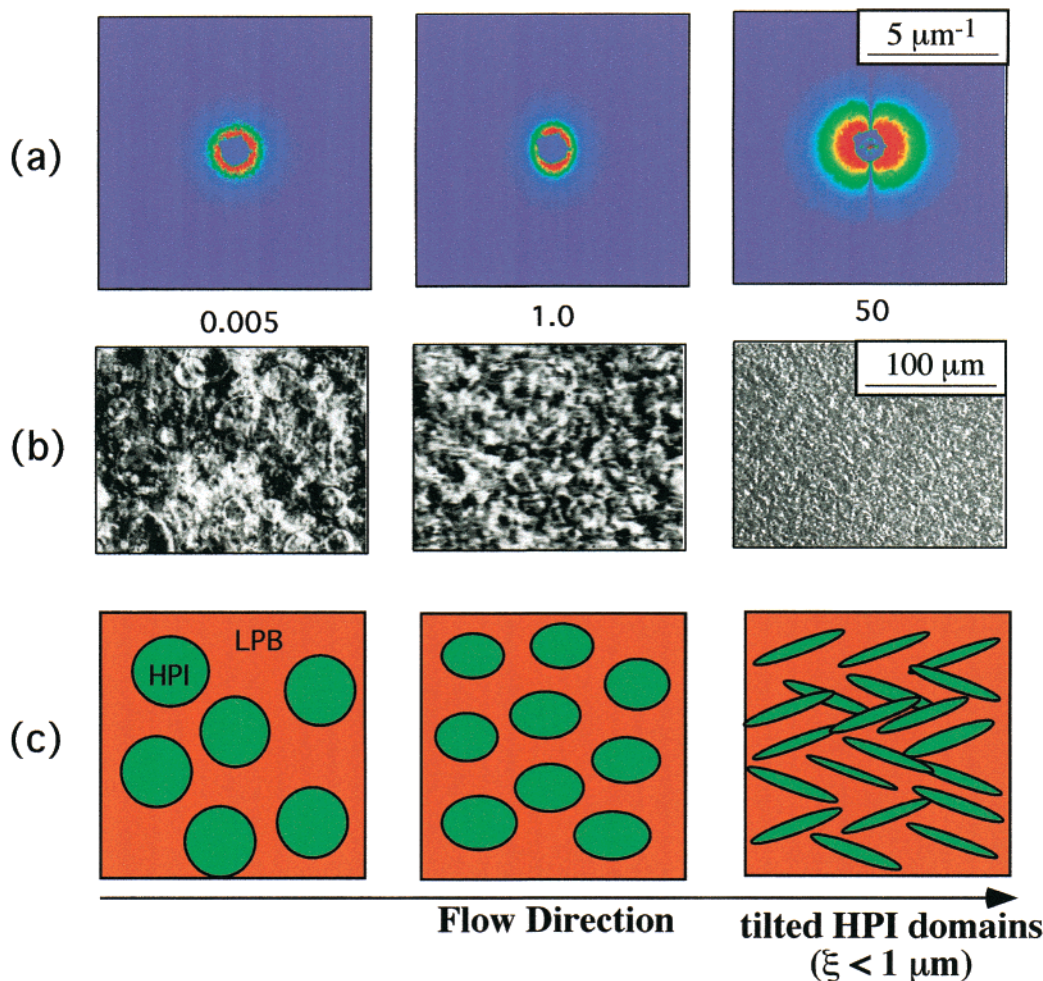


Figure 7. (a) Two-dimensional small-angle light-scattering (SALS) patterns, (b) phase-contrast optical micrographs, and (c) domain morphology cartoons for the A20 blend at 130 °C at various shear rates, where the shear rate in inverse seconds is indicated under each light-scattering pattern. The flow direction is from left to right, and the vorticity direction is from top to bottom.

of domain structures during the 120 min intervals, while samples in the single-phase region appear as featureless, blank images. Figure 1 shows the phase diagram of LPB/LPI, which has a lower critical solution temperature (LCST) of (61.5 ± 0.5) °C. We estimate the spinodal temperature of the upper-critical-solution-temperature (UCST) LPB/HPI blends using the Flory–Huggins interaction parameter (χ) obtained from small-angle-neutron-scattering (SANS) data.²⁵ The estimated critical temperature (at $\phi_{\text{HPI}} = 0.45$) is much greater than 250 °C, the upper limit of the experimental temperature range.

2. Phase-Inversion Composition. Figure 2 shows optical micrographs of phase-separated LPB/LPI blends under quiescent conditions at 130 °C. The dispersed phase appears as polydisperse spherical droplets over a wide range of compositions ($0.1 \leq \phi_{\text{LPI}} \leq 0.8$), with the number-average droplet size depending on the composition of the blends. The LPI-rich droplets ($\phi_{\text{LPI}} < 0.5$) appear lighter than the LPB-rich droplets ($\phi_{\text{LPI}} > 0.6$). However, the difference is not profound because the refractive indices of the two components are almost identical.

In Figure 3, we show the steady shear viscosity versus ϕ_{LPI} , as well as optical micrographs and light-scattering patterns for the blend B40 at shear rates of 0.001 and 0.1 s^{-1} . In Figure 3c and d, the relatively low shear rate ($\dot{\gamma} = 0.001 \text{ s}^{-1}$) does not readily alter the droplet shape. In

Figure 3a, we observe a continuous increase in the blend viscosity as the volume fraction of LPI increases from 0 to 0.6, while the blend viscosity decreases systematically for $\phi_{\text{LPI}} > 0.6$, suggesting that the dispersed phase is inverted from LPI-rich to LPB-rich. In general, the viscosity of a phase-separated binary fluid contains an excess shear viscosity term that arises from the presence of domain interfaces,^{26–28} and thus the viscosity should be somewhat sensitive to changes in morphology. Figure 3b demonstrates that there is a systematic increase in the high-shear viscosity (measured at $\dot{\gamma} = 0.1 \text{ s}^{-1}$) with increasing ϕ_{LPI} in the LPI-rich dispersed phase for $\phi_{\text{LPI}} < 0.55$ or the LPB-rich dispersed phase for $\phi_{\text{LPI}} > 0.55$. As ϕ_{LPI} increases, a discontinuity in η at $\phi_{\text{LPI}} = 0.55$ is evident, suggesting again that the continuous phase is inverted from LPB-rich to LPI-rich. Thus, the phase-inversion composition would be $\phi_{\text{LPI},i} = 0.55 \pm 0.05$ at $\dot{\gamma} = 0.1 \text{ s}^{-1}$.

In Figure 4, we show the compositional dependencies of the dynamic storage modulus (G'), the loss modulus (G'') (both measured at a frequency of 0.1 rad/s), and the mean droplet size (R) for phase-separated LPB/LPI. At this low frequency, a systematic increase in G' with increasing LPI volume fraction (up to $\phi_{\text{LPI}} \sim 0.6$) is evident, indicative of an increase in the concentration and size of

(26) Doi, M.; Ohta, T. *J. Chem. Phys.* **1991**, *95*, 1242.

(27) Onuki, A. *Phys. Rev.* **1987**, *A35*, 5149.

(28) Matsuzaka, K.; Koga, T.; Hashimoto, T. *Phys. Rev. Lett.* **1998**, *80*, 5441.

(25) Hasegawa, H.; Sakurai, S.; Takenaka, M.; Hashimoto, T.; Han, C. C. *Macromolecules* **1991**, *24*, 1813.

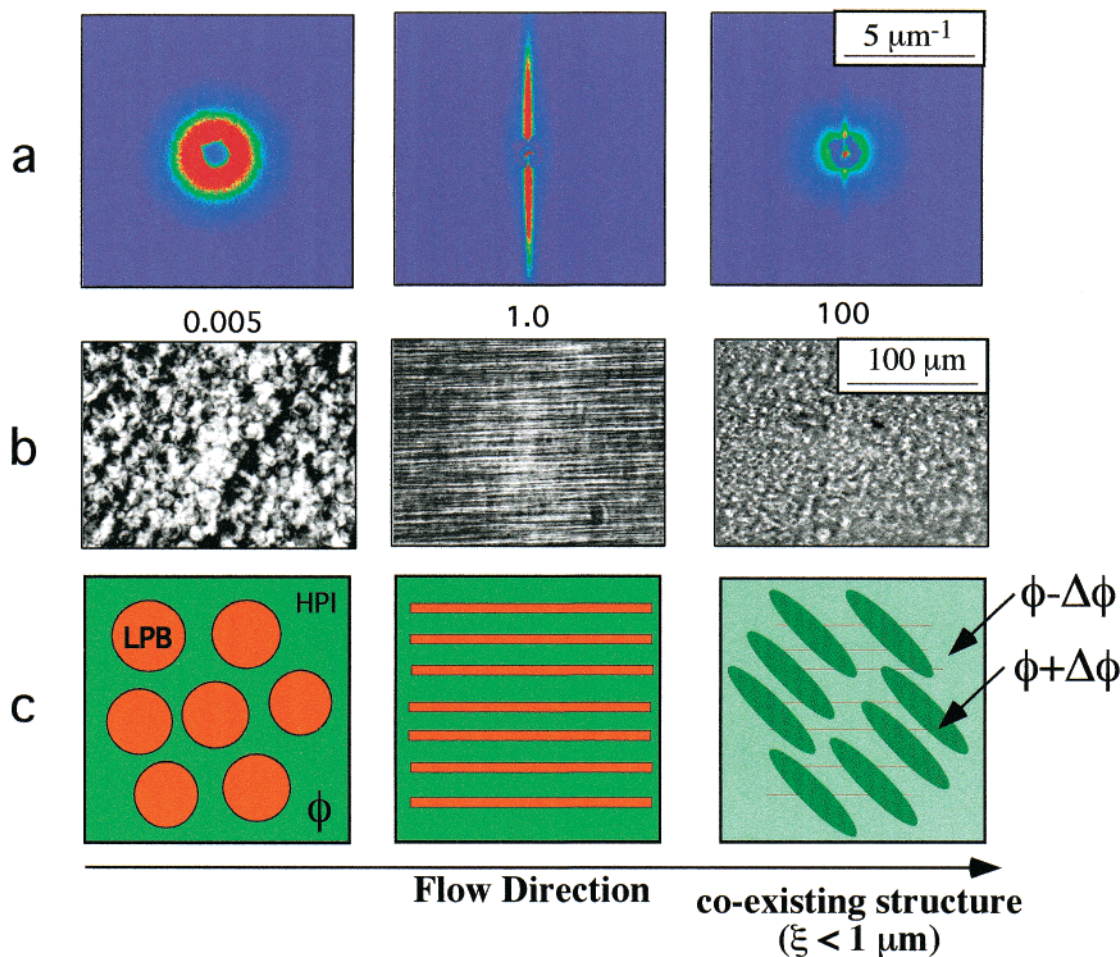


Figure 8. (a) Two-dimensional small-angle light-scattering (SALS) patterns, (b) phase-contrast optical micrographs, and (c) domain morphology cartoons for the A80 blend at 130 °C at various shear rates, where the shear rate in inverse seconds is indicated under each light-scattering pattern. The flow direction is from left to right, and the vorticity direction is from top to bottom.

the LPI-rich droplets. Again, reminiscent of the behavior exhibited by the viscosity at low shear, the storage modulus decreases continuously for $\phi_{\text{LPI}} > 0.6$, suggesting that the dispersed phase is inverted from LPI-rich to LPB-rich. The strong compositional dependence of G' at this low frequency may arise from perturbations to the domain shape under oscillatory shear, which in turn is related to the domain size.^{29,30} In contrast, the compositional dependence of G'' is more or less consistent with a log-additive mixing rule (straight line). We do not observe any discontinuity in the plot of G' versus ϕ_{LPI} .

In Figure 5, we show the compositional dependencies of G' and G'' at a frequency of 10 rad/s for phase-separated LPB/LPI. We observe a continuous increase in G' as the volume fraction of LPI increases, with a discontinuity at $\phi_{\text{LPI}} = 0.55$ suggesting again that the dispersed phase is inverted from LPI-rich to LPB-rich, with the phase-inversion composition $\phi_{\text{LPI},i} = 0.55 \pm 0.05$. The compositional dependence of G'' follows the log-additive mixing rule, suggesting that G'' is well represented by an average contribution from the dispersed and continuous phases.

3. Prediction of Phase-Inversion Composition. The viscosity ratio of LPI/LPB blends ($\lambda = \eta_{\text{LPI}}/\eta_{\text{LPB}}$) is 3 at 130 °C. For $\lambda = 3$, the phase-inversion composition predicted by eq 1 is 0.75, which does not agree with our experimental result ($\phi_{\text{LPI},i} = 0.55 \pm 0.05$). This is probably due to the fact that the viscosity ratio, λ , is significantly larger than

unity. Utracki⁵ has proposed a model that can be used to predict the phase-inversion composition for blends with disparate viscosities:

$$\frac{\eta_A}{\eta_B} = \left(\frac{\phi_m - \phi_A}{\phi_m - \phi_B} \right)^{[\eta]\phi_m} \quad (2)$$

where ϕ_m is the maximum-packing volume fraction and $[\eta]$ is the intrinsic viscosity. For polymer blends, ϕ_m can be taken as $1 - \phi_c$, where ϕ_c is the critical volume fraction for percolation.^{31–33} The theoretical value of ϕ_c for spherical domains is 0.156.^{5,34} The intrinsic viscosity of polymer blends can be estimated from the Oldroyd equation for emulsions³⁴ with the assumption $\eta_p \rightarrow 0$:

$$[\eta] = \frac{2.5\Lambda + 1}{\Lambda + 1} \quad (3)$$

$$\Lambda = (\eta_d + \eta_p)/\eta_c \quad (4)$$

where $[\eta]$ is the intrinsic viscosity of the emulsion, η_c is the viscosity of the continuous phase, η_d is the viscosity of the dispersed phase, and η_p is the viscosity of the

(29) Gramespacher, H.; Meissner, J. *J. Rheol.* **1992**, *36*, 1127.

(30) Vinckier, I.; Moldenaers, P.; Mewis, J. *J. Rheol.* **1996**, *40*, 613.

(31) de Gennes, P. G. In *Percolation Localization and Superconductivity*; Goldman, A. M., Wolf, S. A., Eds.; NATO ASI Series B, Physics, Vol. 109; Plenum Press: New York, 1984.

(32) Stauffer, D. *Introduction to Percolation Theory*; Taylor and Francis: London, 1985.

(33) Grimmett, G. *Percolation*; Springer-Verlag: New York, 1989.

(34) Chapoy, L. J. *J. Chem. Phys.* **1986**, *84*, 1530.

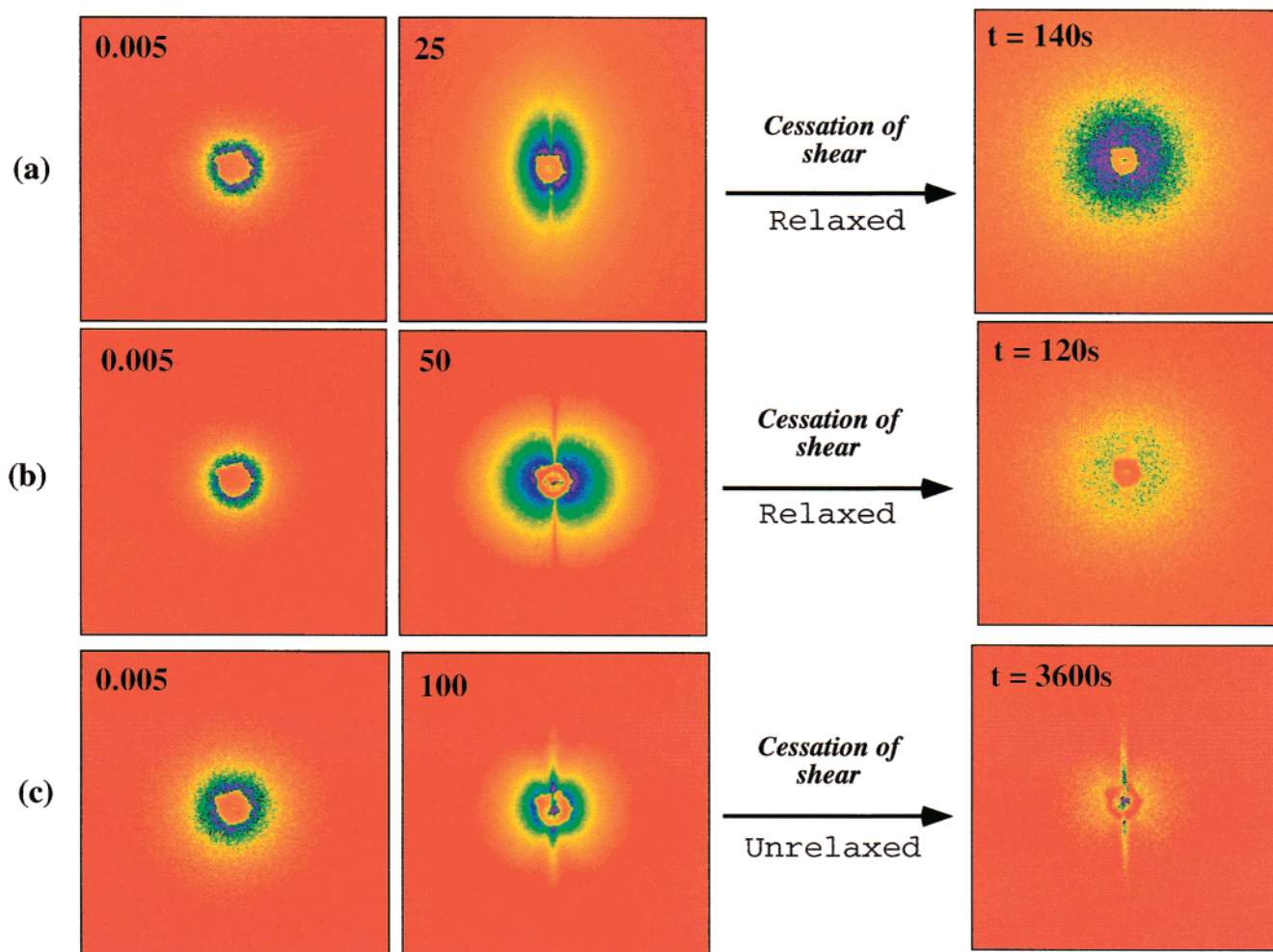


Figure 9. Small-angle light-scattering (SALS) patterns after cessation of shear for three different LPB/HPI blends: (a) A20; (b) A40; (c) A80. The numbers in the upper left corners of the left panels are the initial and final shear rates in units of inverse seconds.

interface. For $\eta_p \rightarrow 0$, the parameter Λ is equal to λ , and the $[\eta]$ value for LPB/LPI at 130 °C calculated from eqs 3 and 4 is equal to 2.125. For $[\eta] = 2.125$ and $\phi_m = 0.844$, the predicted phase-inversion composition for LPB/LPI is 0.6, which is in reasonably good agreement with our experimentally determined value.

4. Shear-Induced Phase Inversion (SIPI). Figure 6 shows two-dimensional small-angle-light-scattering (SALS) patterns, phase-contrast optical micrographs, and morphology cartoons of the B60 blend ($\lambda = 0.33$) at various shear rates (0.005, 1.0, and 100 s^{-1}), where the numbers below the SALS patterns are the shear rates in units of inverse seconds. The patterns shown in Figures 6a and b reveal how the domain morphology gradually evolves from stable, almost-spherical LPB-rich droplets to extended stringlike filaments as the shear rate increases. A stringlike pattern with an extremely high aspect ratio ($\zeta = L/W > 25$, where L and W are the lengths of the domain in the flow and vorticity directions, respectively) appears at a shear rate of 1 s^{-1} . At a shear rate of 100 s^{-1} , a nearly isotropic scattering pattern appears and the micrograph exhibits very little contrast variation, suggestive of shear-induced homogenization at the length scale probed by light-scattering and optical microscopy.

Figure 7 shows two-dimensional SALS patterns, phase-contrast microscopic images, and morphology cartoons for the LPB/HPI (A20) blend ($\lambda = 8.6$) at various shear rates (0.005, 1.0, and 50 s^{-1}). Again, the numbers below the SALS patterns designate the shear rate in units of inverse

seconds. The light-scattering pattern remains almost isotropic until $\dot{\gamma} \sim 1 \text{ s}^{-1}$ and then begins to show a butterfly-like pattern at $\dot{\gamma} = 10 \text{ s}^{-1}$. This scattering pattern, which is characterized by an enhanced scattering along the flow direction but a suppression of scattering along the direction of vorticity, suggests the presence of small (on the order of 1 μm) droplets, with some type of correlated deformation extending (on average) along the vorticity axis. Phase-contrast optical micrographs of the real-space structures that produce these scattering patterns are shown in Figure 7b. The dispersed phase is HPI-rich droplets that deform and decrease in size with increasing shear rate. As the shear rate increases from 0.05 to 1 s^{-1} , the HPI-rich domains become only slightly elongated ($\zeta < 1.5$) due to the relatively high viscosity ratio ($\lambda = 8.6$) of HPI to LPB. For $\dot{\gamma} > 1.0 \text{ s}^{-1}$, the domains break up considerably and become quite small. Measurements of the shear viscosity of the pure components indicate that the HPI starts to exhibit shear thinning at 3 s^{-1} , while the shear viscosity of the LPB does not start to decrease until 100 s^{-1} . Hence, the true viscosity ratio in the breakup regime (around 50 s^{-1}) is much less than 8.6. In general, one would not expect breakup to occur in a blend with a viscosity ratio larger than 4.³⁶ Some anisotropy is apparent, however, in the form of extended correlations in gray scale intensity within an angular sector around the vorticity axis. In Figure 7c,

(35) Oldroyd, J. C. *Proc. R. Soc.* **1955**, A232, 567.

(36) Grace, H. P. *Chem. Eng. Commun.* **1982**, 14, 225.

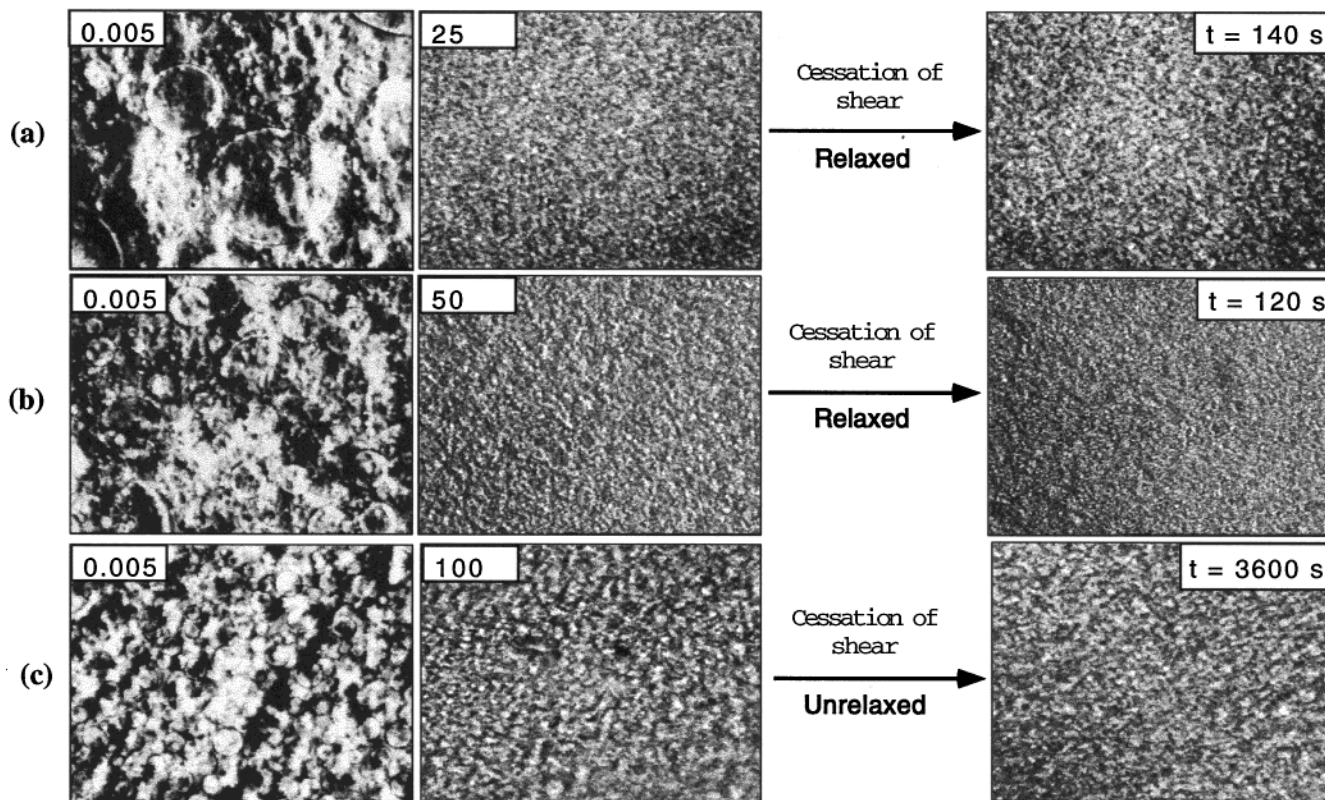


Figure 10. Phase-contrast optical micrographs after cessation of shear for three different LPB/HPI blends: (a) A20; (b) A40; (c) A80. The numbers in the upper left corners of the left panels are the initial and final shear rates in units of inverse seconds. The width of each micrograph is 200 μm . The flow direction is from left to right, and the vorticity direction is from top to bottom.

morphology cartoons describe the overall domain shape under shear flow based on SALS and microscopy results. For the cartoon at $\dot{\gamma} = 50 \text{ s}^{-1}$, the size of the domains is exaggerated to show the tilted orientation with respect to the flow direction, while for simplicity only one orientation is shown.

Figure 8 shows two-dimensional SALS patterns, phase-contrast micrographs, and morphology cartoons for the LPB/HPI (A80) blend at various shear rates (0.005, 1.0, and 100 s^{-1}). The light-scattering patterns shown in Figure 8a are isotropic at the low shear rate of 0.005 s^{-1} . As the shear rate increases, both the SALS patterns and real-space micrographs reveal the formation of stringlike domains, but with a decrease in intensity at around 10 s^{-1} . At 100 s^{-1} , a unique light-scattering pattern with a "walnutlike" shape emerges, which is a superposition of a stringlike pattern and a butterfly-like pattern, suggesting that there are two coexisting structures. The walnutlike pattern is exactly a superposition of the two patterns observed from the LPB-rich droplet and HPI-rich droplet scenarios. The coexistence, therefore, may be explained as a shear-induced phase inversion, in which the matrix component of the HPI-rich phase is converted to the dispersed phase and shows the butterfly-like pattern under high shear. In Figure 8c, the morphology cartoon depicts the domain deformation under shear flow, with the cartoon at $\dot{\gamma} = 100 \text{ s}^{-1}$ showing the coexisting structures: LPB-rich stringlike domains and HPI-rich vorticity-aligned domains (again, only one tilt angle is represented and the scale of the domain structure is exaggerated). The light and dark green represent the low and high concentrations of HPI-rich phases, respectively. The dispersed domains (dark green) represent the shear-induced concentration enhancement ($\phi + \Delta\phi$) with respect to the original concentration (ϕ) of HPI-rich domains, and the matrix (light green) represents the concentration

decrease ($\phi - \Delta\phi$) in the HPI-rich matrix. The butterfly-like scattering pattern that develops in the A80 blend thus appears in conjunction with a coupling between concentration fluctuations and shear stress.³⁷

As further evidence of coexisting structures in the LPB/HPI (A80) blend, we performed cessation of shear experiments at $130 \text{ }^\circ\text{C}$. Figures 9 and 10 show phase-contrast optical micrographs and light-scattering patterns for three blends: (a) A20, (b) A40, and (c) A80. The numbers in the upper left-hand corners represent the initial and final shear rates in units of inverse seconds. At low shear, the mixtures form polydisperse droplets which are HPI-rich in blends a and b but LPB-rich in blend c. In contrast to the behavior observed in a previous study,³⁸ upon further increase in shear rate, blends a and b exhibit butterfly light-scattering patterns (at 25 and 50 s^{-1} , respectively), while blend c exhibits a walnutlike pattern, as discussed above. Upon cessation of shear, blends a and b relax to isotropic patterns with a characteristic time smaller than 140 and 120 s, respectively, while blend c retains its anisotropy on a much longer time scale, 3600 s. The possible implication of this profound difference in relaxation is that it takes much longer for the phase-inverted mixture to relax back to an equilibrium thermodynamic state consisting of droplets of the minority phase dispersed in a matrix of the majority phase. This could have significant implications for the processing of polyolefin blends, for example.

Conclusions

We have determined the phase-inversion compositions of phase-separated LPB/LPI blends on the basis of

(37) Helfand, E.; Fredrickson, G. H. *Phys. Rev. Lett.* **1989**, *62*, 2468.
 (38) Kielhorn, L.; Colby, R. H.; Han, C. C. *Macromolecules* **2000**, *33*, 2486.

discontinuities in the dynamic storage modulus and shear viscosity as a function of composition, and these values are comparable to those predicted from Utracki's model equation. We also observe a coexisting structure that we suggest may be due to shear-induced phase inversion at a fixed composition and constant temperature. This coexisting structure is composed of two different morphologies: stringlike domains and vorticity-elongated domains with a small characteristic length scale ($\xi < 1 \mu\text{m}$). Cessation-of-shear experiments provide further suggestive evidence that this coexisting structure is associated with shear-induced phase inversion. It is interesting to note that a similar type of "walnutlike" scattering pattern, which we attribute to the coexistence of two distinct morphologies, has been observed in another polymer blend system, where it is attributed to a coexistence of unbroken filaments, small droplets, and coalescing droplets.³⁹ Our interpretation, which is based on a cumulative picture of light scattering, microscopy, and

rheology, is not inconsistent with the scenario proposed in ref 39. Rather, we are suggesting that shear-induced phase inversion may lie at the foundation of this coexistence, at least in the system we have studied, pointing to the need for further work, both experimental and theoretical, on this topic.

Acknowledgment. We would like to thank Dr. Adel Halasa and Dr. Bill Hsu (Goodyear Tire and Rubber Company) for synthesis of the polymers used in this study.

Data in graphs and uncertainties in quoted numerical results represent the best estimate of the standard error in experimental uncertainty.

LA001160R

(39) Yang, H.; Zhang, H.; Moldenaers, P.; Mewis, J. *Polymer* **1998**, *39*, 5731. Mewis, J.; Yang, H.; Van Puyvelde, P.; Walker, L. M. *Chem. Eng. Sci.* **1998**, *53*, 2231.